

Research paper

Performance optimization of a mK dilution refrigerator based on the first law of thermodynamics

Yujia Zhai^{a,c}, Haizheng Dang^{a,b,c,d,*}^a State Key Laboratory of Infrared Physics, Shanghai Institute of Technical Physics, Chinese Academy of Sciences, 500 Yutian Road, Shanghai 200083, China^b Shanghai Research Center for Quantum Sciences, Shanghai 201315, China^c University of Chinese Academy of Sciences, Beijing 100049, China^d Shanghai Boreas Cryogenics Co., Ltd, Shanghai 201802, China

ARTICLE INFO

Keywords:

Dilution refrigerator
Performance optimization
Enthalpy flow model
First law of thermodynamics

ABSTRACT

This paper analyzes and optimizes performance characteristics of the dilution refrigerator (DR) based on the first law of thermodynamics. The properties of the ^3He - ^4He mixture below 0.7 K are analyzed and a simplified method to obtain the enthalpy of the working fluid in the whole dilution cycle is proposed. Then an enthalpy flow model is built, based on which the variations of the specific cooling capacity, specific still heating power and gross cooling capacity with the precooling temperature and upstream pressure are studied at the cooling temperature of 10 mK, and the effect of the first-stage heat exchanger efficiency on the gross cooling capacity is further analyzed. The results indicate that there exists an optimal upstream pressure which maximizes the gross cooling capacity for a given precooling temperature. The optimal upstream pressure and the maximum gross cooling capacity are investigated based on the fitting functions of precooling temperatures. Given a heat exchanger efficiency of 97 %, it is found that the optimal upstream pressure and precooling temperature should be 1.41×10^5 Pa and around 4 K, respectively, to achieve the maximum cooling capacity of 38.5 μW at 10 mK. This study provides a helpful theoretical guidance for the performance optimization of the DR.

1. Introduction

In recent years, the rapid development of the quantum information technology, low temperature physics leads to the increasing demand for cryogenic environment at millikelvin temperatures. For instance, studies on the fractional quantum Hall effect (FQHE) [1,2] and topological quantum materials [3] require the low-temperature environment of below 100 mK. And for the superconducting quantum computer, the quantum chip normally operates at below 20 mK [4] to suppress the thermal noise at the energy level of GHz [5].

Compared with other millikelvin refrigerators such as the adiabatic demagnetization refrigerator (ADR) and the adsorption refrigerator (AR), the dilution refrigerator (DR) not only operates continuously and stably but also features the merits of lower vibration and lower electromagnetic interference as well. In addition, the cooling capacity of the DR is much higher than that of the ADR. For instance, the ADR usually reaches 30–35 μW at 100 mK [6] while the DR can even achieve 850–1000 μW at 100 mK [7,8]. The high cooling capacity of the DR

offsets the heat losses of the coaxial and electrical lines, which makes it the most promising candidate in the quantum information technology.

The DR achieves the cooling temperature by utilizing the phase separation characteristic of the ^3He - ^4He mixture at 0.86 K and the endothermic entropy-increasing process of ^3He from the concentrated phase (*c*-phase) to the dilute phase (*d*-phase). At present, there already exist several commercial products of DRs, and a few of theoretical studies about the dilution cycle have been reported. For example, Wheatley et al. [9,10] compared different types of DRs and qualitatively analyzed the intrinsic factors that hindered the refrigeration performance. Radebaugh et al. [11,12], Lounasmaa [13], and Frossati [14] focused on the analysis of various heat exchangers to optimize the cooling performance. Pradhan et al. [15,16] built a numerical simulation model and discussed the variation of the cooling capacity with the flow rate and purity of working fluid under the steady state conditions. Chaudhry et al. [17] investigated the cooling performance of a gravity-insensitive dilution refrigerator. Mueller et al. [18] built a thermodynamic model of a DR without mechanical drive components and optimized the structural parameters to improve the performance.

* Corresponding author at: State Key Laboratory of Infrared Physics, Shanghai Institute of Technical Physics, Chinese Academy of Sciences, 500 Yutian Road, Shanghai 200083, China.

E-mail address: haizheng.dang@mail.sitp.ac.cn (H. Dang).

<https://doi.org/10.1016/j.cryogenics.2023.103731>

Received 26 July 2023; Received in revised form 19 August 2023; Accepted 24 August 2023

Available online 25 August 2023

0011-2275/© 2023 Elsevier Ltd. All rights reserved.

Nomenclature			
A	area (m^2)	s	specific entropy (J/mol K^{-1})
CHEX	counterflow heat exchanger	T_M	temperature of the MC (mK)
C	molar specific heat (J/mol K^{-1})	T_S	temperature of the still (K)
d	orifice diameter (μm)	T_{pre}	precooling temperature (K)
DHEX	discrete heat exchanger	T_W	warm end temperature (K)
g	molar gibbs free energy (J/mol)	T_C	cold end temperature (mK)
G	molar mass flux ($\text{mol m}^{-2} \text{s}^{-1}$)	V_4	^4He partial molar volume (m^3/mol)
h	specific enthalpy (J/mol)	x	concentration
h_3^0	specific enthalpy of pure ^3He	<i>Greeks</i>	
M	molecular mass (g/mol)	η	efficiency of CHEX
MC	mixing chamber	κ	ideal gas ratio of isobaric to isochoric heat capacities
\dot{n}	molar flow rate ($\mu\text{mol/s}$)	μ	chemical potential (J/mol)
P_U	inlet upstream pressure (Pa)	<i>Cyril</i>	
P_H	high pressure after the J-T valve (Pa)	Π	osmotic pressure (Pa)
P_D	downstream pressure above the still (Pa)	<i>Subscripts</i>	
P_L	low pressure of the dilute phase (Pa)	0	stagnation conditions
PHEX	precooling heat exchanger	1,2,3...	thermodynamic states in Fig. 2
q_M	specific cooling capacity in the MC (J/mol)	c	concentrated
q_S	specific heating power in the still (J/mol)	d	dilute
Q_M	cooling capacity in the MC (μW)	l	low concentration
Q_S	heating power in the still (mW)	m	mixture
R	universal gas constant ($8.314 \text{ J mol}^{-1} \text{ K}^{-1}$)	opt	optimal

However, the previous theoretical research mainly focused on the optimization of structure parameters and on the relationships between the flow rate, cooling temperature and cooling capacity. For in-depth performance optimization, the comprehensive analysis of the influence of both the inlet operating condition and the heat exchanger efficiency is required. This paper will conduct the investigation on the performance analysis and optimization of the DR based on the first law of thermodynamics. Since the ^3He - ^4He mixture exists below the still in the DR, the thermodynamic properties of the liquid mixture will be first calculated. Then an enthalpy flow model will be built, and then the variations of both specific and gross cooling capacities with precooling temperature and upstream pressure at the cooling temperature of 10 mK with a perfect heat exchanger will be investigated. The effects of the heat exchanger efficiency will then be discussed, and finally the working mechanism of the DR is clarified and the systematic optimization of its cooling capacity will be summarized.

2. The ^3He - ^4He mixture in the DR

2.1. The characteristic of the ^3He - ^4He mixture

The working fluid of the DR is the ^3He - ^4He mixture. Since the mixture is divided into the c -phase and d -phase of ^3He in both the still and the mixing chamber, the component and state vary with the temperature in the whole refrigeration cycle.

As shown in Fig. 1, the phase separation of the ^3He - ^4He mixture occurs at 0.86 K. The red curve in Fig. 1 represents the c -phase saturation curve while the blue one is the d -phase one. With the decreasing temperature, the concentration of c -phase x_c gradually increases to 100 % while that of d -phase x_d goes to 6.4 %, and thus the c -phase can be regarded as pure ^3He at the extremely-low temperatures. Therefore, the relatively complicated d -phase will be focused on.

Radebaugh [19] utilized the weak interaction Fermi gas model of ^3He in ^4He to carry out the calculation of the thermodynamic properties of the mixture with the ^3He concentration of lower than 30 % at below 1.5 K. Kuerten et al. [20] calculated the properties of the mixture confined to the ^3He concentration lower than 8 % and the temperature below 0.25 K starting from the experimental values of the molar volume,

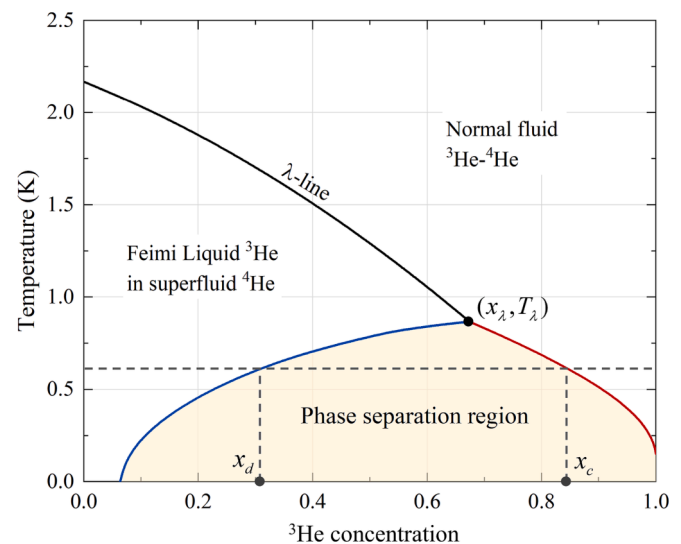


Fig. 1. Phase diagram of the ^3He - ^4He mixture.

the specific heat, and the osmotic pressure. Chaudhry et al. [21,22] built a model to calculate the properties of liquid ^3He - ^4He mixture at up to 10 bar and below 1.5 K, which was suitable for the superfluid J-T refrigerator [23] operating at higher pressure and employing mixture of higher concentration rather than the DR.

Assuming there is no ^4He evaporation from the still, ^3He is the main cycling fluid during the steady operation of the DR. To overcome the abovementioned limitations, the methods to obtain the enthalpy at below 0.7 K (the typical temperature of the still) in the dilution cycle are discussed in this paper, and the results are shown in Section 2.5 based on the calculated values of the osmotic pressure in Section 2.4, which plays a key role in the theoretical analysis in the DR based on the first law of thermodynamics.

2.2. The cooling progress of the DR

Fig. 2 shows a simplified schematic of the DR, which is composed of a precooling unit driven by a compressor and a dilution unit driven by an external pumping unit. The dilution unit consists of the first-stage counterflow heat exchanger (CHEX), the J-T valve, the still, the second-stage CHEX, the discrete heat exchanger (DHEX), and the mixing chamber (MC).

The pressure of the working fluid is lifted by various types of pumps stage by stage, from P_D to P_U . The upstream ^3He flow with molar flow rate \dot{n} enters the system and is precooled to T_1 by two PHEXs. Then it exchanges heat with the downstream ^3He vapor and passes through the J-T valve. In this process, the pressure decreases from P_U to P_H , after which the high-pressure ^3He flow is further cooled and achieves complete liquefaction in the coil immersed in the ^3He - ^4He liquid mixture in the still. Simultaneously, the liquid mixture is heated by the inlet high-pressure flow and the external heater to get ^3He vapor. After the pure ^3He liquid passes through two types of heat exchangers (CHEX and DHEXs) and is cooled down to T_6 , it finally enters the MC where the d -phase mixture driven by the concentration gradient from the still to the MC leaves and the ^3He in the c -phase passes through the phase interface

to produce a corresponding temperature drop due to the increasing entropy. Furthermore, to recover the cooling capacity from the outlet of the dilution unit to the inlet of the first pump, the low-pressure ^3He vapor from the still also cools the cold plate by the PHEXs.

2.3. Methods to calculate the enthalpy of the mixture

Since the saturated vapor pressure of ^3He in the d -phase is much higher than that of ^4He in the still, ^3He first evaporates into the pump line, and the pipeline above the still is full of pure ^3He gas (assuming there is no ^4He evaporation). The so-called ‘ d -phase mixture’ only exists in the pipeline from the MC outlet to the still inlet. Therefore, the inlet and outlet of the heat exchangers between them are regarded as the control volume in this section and the enthalpy differences of both the c -phase and d -phase are compared to find the most appropriate method to calculate the enthalpy of the mixture.

For the c -phase, enthalpy difference under the steady state operation is expressed as:

$$\Delta h_c = h_3^0(P_H, T_w) - h_3^0(P_H, T_c) \quad (1)$$

where P_H is the pressure of the c -phase pipeline after the J-T valve. h_3^0

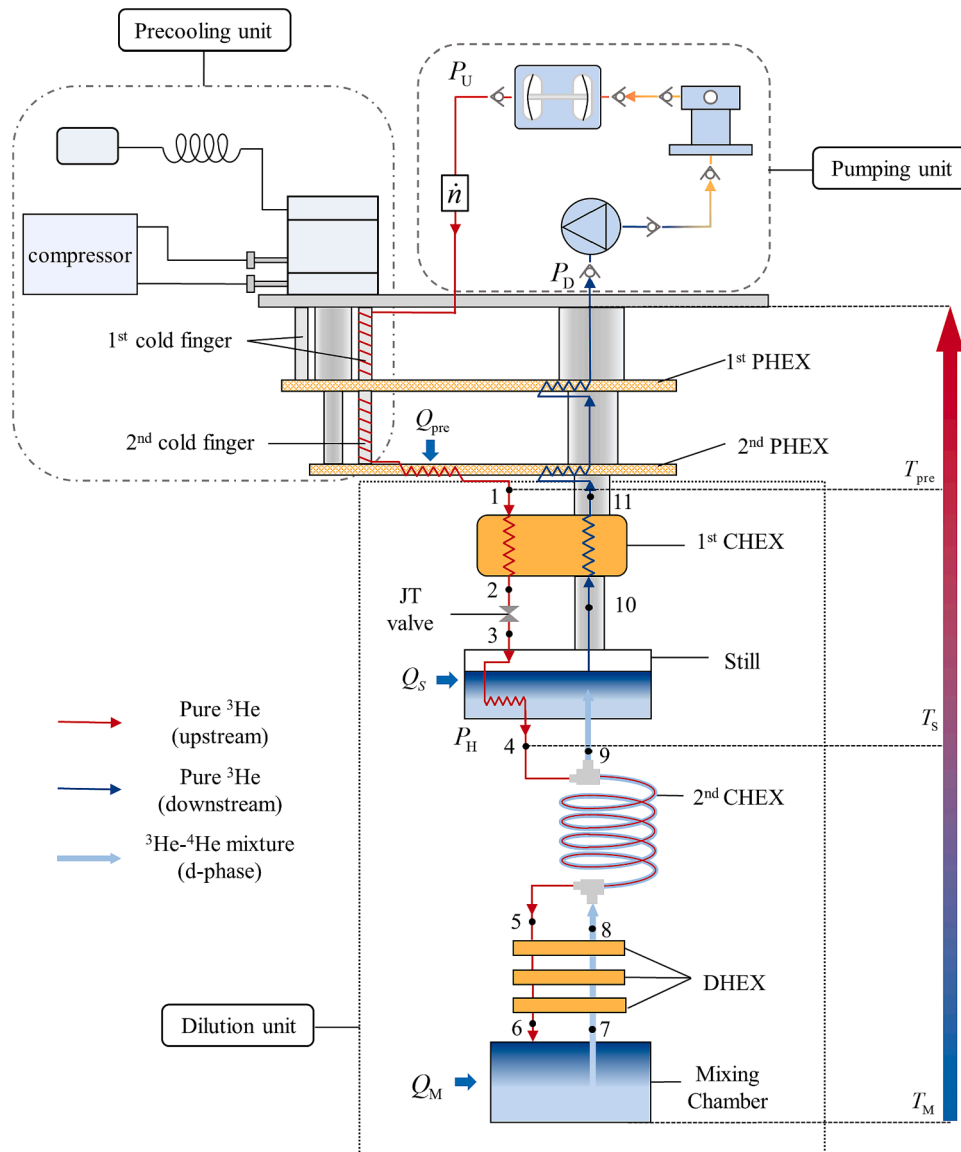


Fig. 2. A simplified schematic of the dilution refrigerator.

is the enthalpy of pure ^3He . T_W and T_C are the warm and cold end temperatures of the heat exchangers, respectively. The pressure drop is ignored here to simplify the calculation.

For the d -phase, the following three methods are summarized for calculating the enthalpy difference:

(a) The inlet and outlet temperature are fixed, the pressure drop on the low-pressure side is ignored, and the mixture is saturated liquid. With the calculated enthalpy of the mixture, the enthalpy difference between the inlet and outlet is:

$$\Delta h_{d1} = h_m(P_L, T_W, x) - h_m(P_L, T_C, x) = h_m(0, T_W, x) - h_m(0, T_C, x) \quad (2)$$

where P_L is the pressure of the d -phase between the MC and still and x is the ^3He concentration. h_m is the enthalpy of the mixture.

(b) The inlet and outlet temperature are fixed, the pressure drop on the low-pressure side is ignored, and the mixture is saturated liquid. Since the existence of osmotic pressure of the ^3He - ^4He mixture, the concept of osmotic enthalpy is proposed. The enthalpy difference between the inlet and outlet is:

$$\Delta h_{d2} = h_{os}(P_L, T_W, x) - h_{os}(P_L, T_C, x) = h_{os}(0, T_W, x) - h_{os}(0, T_C, x) \quad (3)$$

where h_{os} refers to the osmotic enthalpy of the mixture.

(c) The d -phase mixture is regarded as the ^3He flowing in the ^4He environment while the osmotic pressure of ^3He in ^4He as the static pressure. The enthalpy value of ^3He is obtained according to the calculated osmotic pressure and the enthalpy difference of the d -phase is:

$$\begin{aligned} \Delta h_{d3} &= h_3^0(\Pi + P_L, T_W) - h_3^0(\Pi + P_L, T_C) \\ &= h_3^0(\Pi(T_W, x) + 0, T_W) - h_3^0(\Pi(T_C) + 0, T_C) \end{aligned} \quad (4)$$

where Π is the osmotic pressure of ^3He in ^4He .

Fig. 3 shows the comparison between the enthalpy difference of the c -phase and d -phase based on methods (a), (b), and (c) at various warm end temperatures when $x = 7\%$. It is obvious that the results of method (c) are always the closest to those of the c -phase while those of the other two methods deviate a lot. In particular, the enthalpy difference calculated by method (b) is about 6 times that of the c -phase, which is quite unreasonable. The units of the c -phase and the d -phase cannot be unified simply by dividing the molar concentration x due to the interaction between molecules in the mixture, so this paper adopts the method (c) to calculate the enthalpy of the dilution cycle. The basis of this method is the calculation of the osmotic pressure.

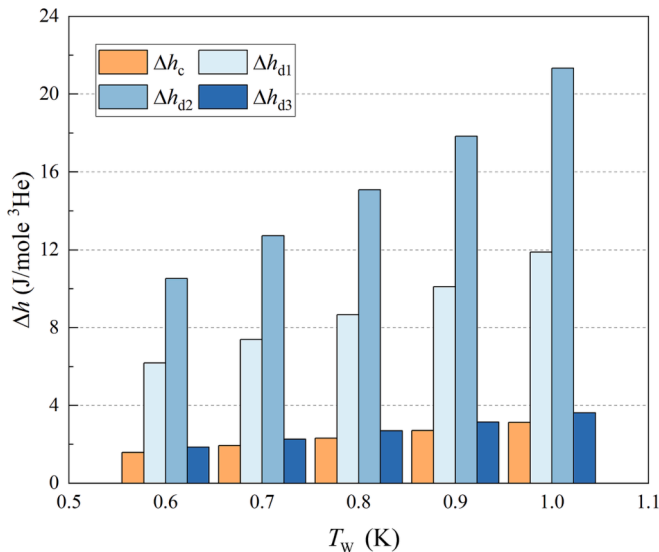


Fig. 3. Comparisons of enthalpy differences of c -phase and d -phase calculated by methods (a), (b), and (c) at various warm end temperatures.

2.4. The osmotic pressure of the ^3He - ^4He mixture

The osmotic pressure at below 250 mK was given by Kuerten et al. [20], while the Gibbs free energy of the mixture above 250 mK can be expressed as [21]:

$$g_m(x, T) = h_l(x) - Ts_l(x) + \int_{T_l(x)}^T C_m(x, T) dT - T \int_{T_l(x)}^T \frac{C_m(x, T)}{T} dT \quad (5)$$

where

$$h_l(x) = h(x, 0.15 \text{ K}) \quad (6)$$

$$s_l(x) = s(x, 0.15 \text{ K}) \quad (7)$$

$$T_l(x) = 0.15 \text{ K} \quad (8)$$

$$C_m(x, T) = xC_3^0(T) + (1-x)C_4^0(T) + x(1-x)C_r(x, T) \quad (9)$$

According to the thermodynamic equation, the chemical potential of ^3He and the molar entropy of the mixture are given by:

$$\mu_3 = g + (1-x) \left(\frac{\partial g}{\partial x} \right)_T \quad (10)$$

$$s_m = - \left(\frac{\partial g}{\partial T} \right)_P \quad (11)$$

The osmotic pressure can be determined as [24]:

$$\mu_4(P, T, x) = \mu_4(P - \Pi, T, 0) \quad (12)$$

$$\Pi(T, x) = \frac{\mu_4(T, x) - \mu_4^0(T)}{V_4(x)} \quad (13)$$

where $V_4(x) = 27.58 - 3.3x^3$ is the partial molar volume of ^4He slightly different from the molar volume of pure ^4He , μ_4 is the chemical potential of ^4He in the mixture and μ_4^0 is the chemical potential of pure ^4He .

The Gibbs-Duhem function of the d -phase mixture at constant pressure is:

$$x d\mu_3(T, x) + (1-x) d\mu_4(T, x) = -s_m(T, x) dT \quad (14)$$

where μ_3 , μ_4 are the chemical potential of ^3He and ^4He in the mixture, respectively. Both are functions of x and T . s_m is the molar entropy of the mixture. Equation (14) can be written as:

$$x \left[\left(\frac{\partial \mu_3}{\partial x} \right)_T dx + \left(\frac{\partial \mu_3}{\partial T} \right)_x dT \right] + (1-x) \left[\left(\frac{\partial \mu_4}{\partial x} \right)_T dx + \left(\frac{\partial \mu_4}{\partial T} \right)_x dT \right] = -s_m dT \quad (15)$$

The Gibbs-Duhem function of the mixture at constant temperature and pressure is:

$$x d\mu_3(x) + (1-x) d\mu_4(x) = 0 \quad (16)$$

So Eq. (15) can be simplified as:

$$x \left(\frac{\partial \mu_3}{\partial T} \right)_x + (1-x) \left(\frac{\partial \mu_4}{\partial T} \right)_x = -s_m \quad (17)$$

Eq. (17) is integrated from 0 to T and then becomes:

$$\mu_4(T, x) - \mu_4^0(T) = - \int_0^T \frac{1}{1-x} s_m(T', x) dT' - \int_0^T \frac{x}{1-x} \left(\frac{\partial \mu_3(T', x)}{\partial T'} \right)_x dT' \quad (18)$$

Based on the above analyses, given the molar entropy of the mixture and the ^3He chemical potential, the osmotic pressure of the d -phase mixture at above 250 mK can be deduced according to Eqs. (13) and (18).

Fig. 4 shows the relationship between osmotic pressure and temperature at different concentrations. The osmotic pressure is

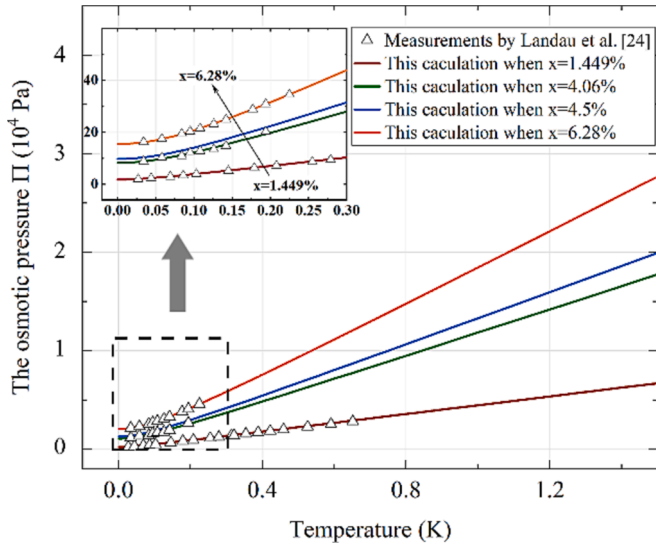


Fig. 4. Relationship between osmotic pressure and temperature at different concentrations.

proportional to either temperature or concentration. The experimental values of the osmotic pressure given by Landau et al. [24] fit the results well, thereby validating the correctness of this method.

2.5. The enthalpy applied to the dilution refrigerator

The enthalpy of the ^3He - ^4He mixture on the low-pressure side at below 0.7 K (the typical temperature of the still) can be obtained using the calculated osmotic pressure at above 250 mK in Section 2.4. Combined with the enthalpy of ^3He gas on the low-pressure side at above 0.7 K and c -phase on the high-pressure side in the entire temperature range, a series of enthalpies which can be applied in the thermodynamics analysis of the DR are obtained.

Fig. 5 shows the enthalpies of the concentrated and dilute phases in different components. With the pressure drop being ignored, the dilution cycle involves different pressure segments on the dilute and concentrated sides due to the J-T valve as well as the phase transition in the still. Point ‘a’ refers to the upstream inlet pressure P_U before the J-T valve, point ‘b’ is the pressure of the c -phase P_H after the J-T valve, point

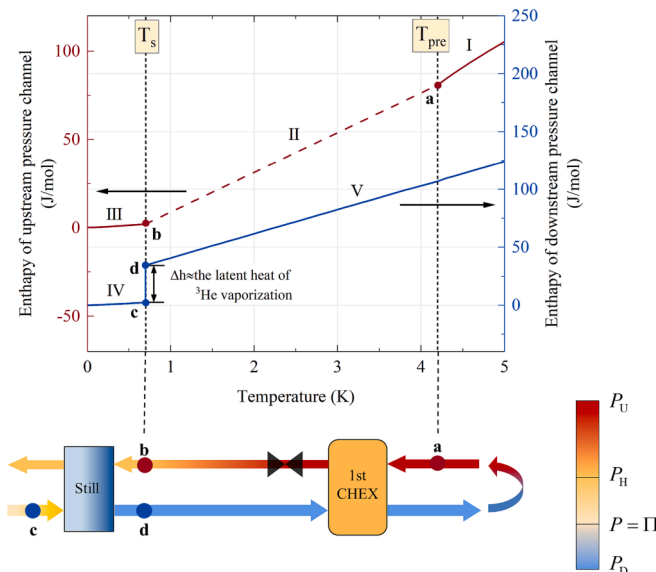


Fig. 5. Enthalpy of concentrated and dilute phases in different components.

‘c’ represents the static pressure of the d -phase mixture equal to the osmotic pressure of ^3He in ^4He in Section 2.3, and point ‘d’ is the saturation vapor pressure of ^3He . There are also various processes in different pressure segments: I is the precooling process of the c -phase, and the pressure stays constant at P_U , II is the cooling process of the c -phase in the first-stage CHEX and the J-T valve (indicated by the dotted line in Fig. 4 considering the simultaneously changing pressure), III is the liquefaction and cooling process of the c -phase between the still and the MC where the pressure keeps constant at P_H , and IV is the endothermic process of the d -phase liquid mixture in the heat exchangers below 0.7 K where the pressure is the osmotic pressure which is proportional to temperature, and V is the endothermic process of the pure ^3He gas in the J-T heat exchanger. It should be noted that the enthalpy difference between points ‘b’ and ‘c’ approximates the latent heat of ^3He vaporization.

The enthalpy of each state in the dilution cycle can be calculated by the above model, which plays an essential role in the following theoretical analysis based on the first law of thermodynamics.

3. The enthalpy flow model of the dilution refrigerator

3.1. Assumptions

The following assumptions are made to simplify the analysis:

- (1) P_U , P_H , and P_D keep constant in the dilution cycle, indicating that the pressure drop in each section is ignored.
- (2) The J-T effect of the dilution cycle all comes from the J-T valve, and the J-T heat exchanger is regarded as the first-stage CHEX. Since the internal process of throttling is not discussed in this paper, it is assumed that the J-T valve can meet all requirements of different operating conditions in the following analysis.
- (3) The second-stage CHEX and the DHEXs are viewed as a whole, and the heat leakage of all the heat exchangers is ignored.
- (4) The inlet temperature of the working fluid is equal to the pre-cooling temperature, that is, $T_1 = T_{pre}$.

The saturated vapor pressure of ^3He corresponding to the still temperature of 0.7 K is about 179 Pa [25]. The pressure drop on the downstream pure ^3He side cannot be ignored in the actual DR. However, the influence of hPa-class pressure drop on the enthalpy of the downstream ^3He flow is negligible. For instance, when the pressure decreases from 179 to 9 Pa, the variation of ^3He enthalpy is about 1.2×10^{-5} J/s at the flow rate of 100 $\mu\text{mol/s}$. Besides, this situation can also be improved by increasing the diameter of the pumping pipe. Thus, it is reasonable to ignore the pressure drop on the downstream ^3He side in the following analysis.

3.2. Theoretical analysis based on the first law of thermodynamics

Enthalpy is a crucial parameter because it is closely related to the cooling capacity of the DR. The specific cooling capacity in the MC is defined as:

$$q_M = \frac{Q_M}{\dot{n}} = h_7 - h_6 \quad (19)$$

where Q_M is the gross cooling capacity with the unit of μW and \dot{n} is the molar flow rate with the unit of $\mu\text{mol/s}$.

According to the law of energy conversion, the exchanged heat in both CHEX and DHEXs is expressed as:

$$\delta h = h_4 - h_6 = h_9 - h_7 \quad (20)$$

Based on the first law of thermodynamics, the energy conservation equation in the still can be written as:

$$q_S + (h_3 - h_4) = h_{10} - h_9 \quad (21)$$

Since the throttling process is isenthalpic, we have:

$$h_2 = h_3 \quad (22)$$

The efficiency of the first-stage CHEX is defined as:

$$\eta = \frac{h_{11} - h_{10}}{h_{1D} - h_{10}} = \frac{h_1 - h_2}{h_{1D} - h_{10}} \quad (23)$$

where h_{1D} is the enthalpy at the same temperature as h_1 on the downstream low-pressure side.

Hence, h_3 is determined by:

$$h_3 = h_2 = h_1 - \eta(h_{1D} - h_{10}) \quad (24)$$

According to Eqs. (20)–(22), the following equations can be achieved:

$$h_4 = h_9 - h_7 + h_8 = q_S - h_{10} + h_9 + h_3 \quad (25)$$

The specific still heating power is given as:

$$q_S = (h_{10} - h_9) - (h_2 - h_4) \quad (26)$$

Combining Eqs. (19), (24), and (25), the specific cooling capacity is:

$$q_M = h_9 - h_4 = h_{10} - h_3 - q_S = h_{10} - h_1 + \eta(h_{1D} - h_{10}) - q_S \quad (27)$$

In Eqs. (27), h_{10} is related to the temperature of the still (T_S) and the corresponding saturated vapor pressure while h_1 is determined by P_U and T_{pre} . h_{1D} is the enthalpy at the same temperature as h_1 on the downstream low-pressure side, which involves P_D and T_{pre} . q_S is influenced by the combination of the enthalpy difference of the c -phase between the inlet and outlet of the coil inside the still and the enthalpy of the d -phase entering the still. The former is determined by η , P_U , and T_{pre} , and the latter is by T_M , T_S and x_d . Based on the calculation in Section 2.4, the enthalpy of the d -phase below 0.7 K is given as:

$$h_d(T_S \leq 0.7 \text{ K}) = h_3^0(T_S, \Pi(x_d(T_M), T_S)) \quad (28)$$

The relationship between the concentration and the temperature of the MC can be obtained by fitting the data from the past experimental data [26,27]:

$$x_d(T) = \sum_{i=0}^4 a_i T^i \quad (29)$$

where the coefficient values are shown in Table 1.

Therefore, the specific still heating power and the specific cooling capacity are implicit compound functions of P_U , P_D , T_{pre} , T_M , T_S , and η , as shown as follows:

$$q_S = f_1(P_U, T_{pre}, T_M, T_S, \eta) \quad (30)$$

$$q_M = f_2(P_U, P_D, T_{pre}, T_S, f_1(P_U, T_{pre}, T_M, T_S, \eta), \eta) \quad (31)$$

The gross cooling capacity is:

$$Q_M = \dot{n} \bullet q_M \quad (32)$$

Hence the molar flow rate of the DR is another significant element determined by the J-T valve, the pump unit, and the inflating volume. Since the investigation in this paper is mainly focused on the first law of thermodynamics, we assume that the inflating volume is fixed, and the pump unit can achieve the required flow rate. In previous studies, the molar flow rate was generally regarded as a given value, but it is a complicated function of the inlet condition.

Table 1
Coefficients of Eqs. (29), (44), (45).

	$i = 0$	$i = 1$	$i = 2$	$i = 3$	$i = 4$
a_i	0.05574	0.2675	-0.4402	1.068	—
b_i	-9350	-3587	1.639×10^4	-1526	—
c_i	-147	156.4	-0.001808	-32.01	0.000625

Fig. 6 shows the throttling process of pure ^3He in the c -phase from point 2 to point 3 (see Fig. 2), where the fluid is compressible and the stagnation state is equivalent to the state at the inlet boundary due to the ultra-low flow rate before throttling, namely:

$$P_0 = P_U \quad (33)$$

$$T_0 = T_2 \quad (34)$$

The mass flow rate of the ideal gas throttling process is determined by [28]:

$$G(T_0, P_0) = \frac{\dot{n}}{A} = \kappa^{1/2} \left(\frac{2}{1 + \kappa} \right)^{\frac{\kappa+1}{2(\kappa-2)}} \frac{P_0}{\sqrt{MRT_0}} \quad (35)$$

where A is the minimum cross section area, which is given as:

$$A = \frac{1}{4} \pi d^2 \quad (36)$$

Thus, the gross cooling capacity is expressed as:

$$Q_M = \frac{1}{4} \pi d^2 G(T_0, P_0) q_M = \frac{1}{4} \pi d^2 G(T_2, P_U) q_M \quad (37)$$

where T_2 is also determined by the upstream conditions, such as P_U and T_{pre} , and the efficiency of the first-stage CHEX. The impact of the flow rate can be transferred into that of P_U , T_{pre} , and η .

To sum up, the gross cooling capacity is an implicit functions of P_U , P_D , T_{pre} , T_S , T_M , η , d :

$$Q_M = F\{f_2[P_U, P_D, T_{pre}, T_S, f_1(P_U, T_{pre}, T_M, T_S, \eta), \eta], \dot{n}(P_U, T_{pre}, \eta, d)\} \quad (38)$$

Based on the normally required flow resistance of the J-T valve in the DR, a suitable orifice diameter is determined to be 20 μm . In Sections 4.1, 4.2 and 4.3, the effects of P_U , T_{pre} and η on the specific cooling capacity, specific heating power, and the gross cooling capacity are discussed when $T_M = 10 \text{ mK}$ and $T_S = 0.7 \text{ K}$, namely:

$$q_S = f_1(P_U, T_{pre}, \eta) \quad (39)$$

$$q_M = f_2(P_U, T_{pre}, f_1(P_U, T_{pre}, \eta), \eta) \quad (40)$$

$$Q_M = F\{f_2[P_U, T_{pre}, f_1(P_U, T_{pre}, \eta), \eta], \dot{n}(P_U, T_{pre}, \eta)\} \quad (41)$$

4. Discussions on effects of key parameters

4.1. Effects of upstream pressure

Fig. 7 shows the steady flow process of the c -phase and d -phase in the first-stage CHEX, the J-T valve, and the still, indicating the variation of q_S with P_U when $T_{pre} = 4.2 \text{ K}$. Section 1-2 represents the recuperative cooling process in the first-stage CHEX while section 2-3 is the isenthalpic expansion process through the J-T valve and section 3-4 refers to the cooling process in the still. Section 9s-10 stands for the ^3He endothermic evaporation process in the still, and section 10-11 is the

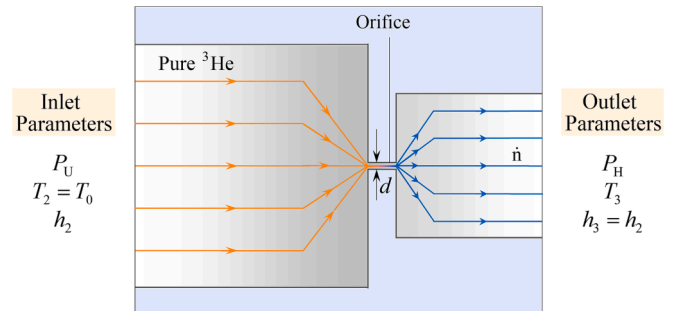


Fig. 6. Throttling process of pure ^3He in the c -phase from point 2 to point 3 (see in Fig. 2).

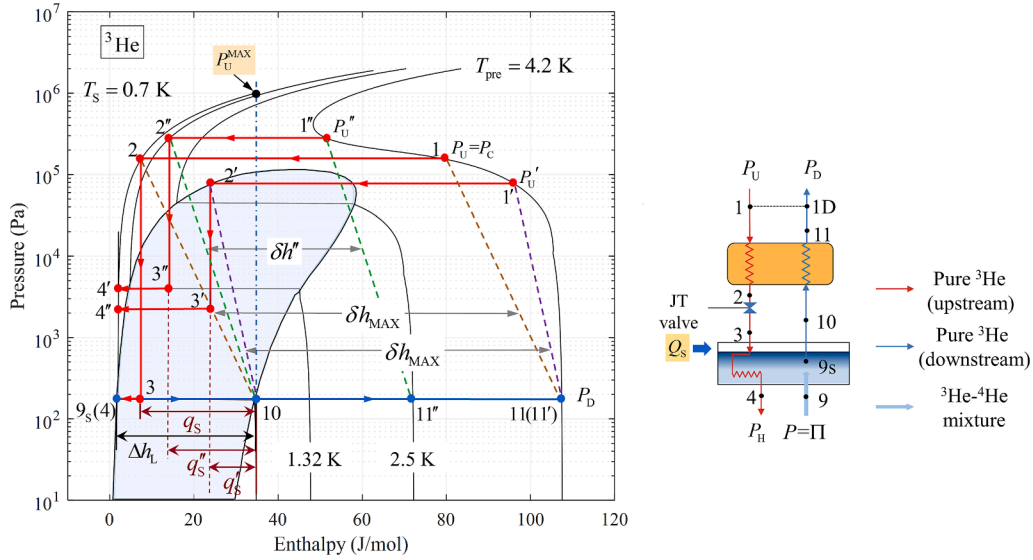


Fig. 7. Steady flow process of the *c*-phase and *d*-phase in the first-stage CHEX, the J-T valve, and the still shown in the *h*-*p* diagram of ³He.

recuperative heating process of the ³He gas in the first-stage CHEX. It is worth noting that point 9s replaces point 9 because the working fluid at point 9 is the mixture of ³He-⁴He which cannot be represented on the *h*-*p* diagram of ³He. Besides, point 1D represents the state at the same temperature as that of point 1 but on the downstream side.

When T_{pre} is 4.2 K, T_s is 0.7 K, and T_M is 10 mK, to investigate the specific cooling capacity and the specific heating power, it is necessary to discuss the state of the outlet of the first-stage CHEX (point 2) as follows:

As shown in Fig. 7, when $P_U > P_C$, the efficiency of the first-stage CHEX is bound to be less than 100%. In this case, the states of working fluid before and after throttling expansion are subcooled liquid and gas-liquid mixture in two-phase region of *h*-*p* diagram, respectively. Under the same upstream pressure, the state of point 2 is also relevant to the efficiency of the heat exchanger that should be considered in the later analysis. On the other hand, when $P_U < P_C$, the efficiency can theoretically reach 100% so the first-stage CHEX is assumed as a perfect heat exchanger. In this case, the states of working fluid before and after throttling expansion are commonly both gas-liquid mixtures in the two-phase region. The corresponding P_U to the precooling temperature of 4.2 K is 1.518×10^5 Pa.

Fig. 8 shows the relationship between the inlet upstream pressure and the heat exchange capacity of the first-stage CHEX, demonstrating that the actual heat exchange capacity is up to that on the low-pressure side when $P_U < P_C$ while up to that on the high-pressure side when $P_U > P_C$, namely:

$$q_{HEX} = \min[(h_1 - h_2), \delta h_{MAX}] \quad (42)$$

$$\delta h_{MAX} = h_{1D} - h_{10} \quad (43)$$

4.1.1. q_M and q_C

Previous studies [29–31] provided the typical values of the upstream pressure and post-throttling temperature. The range of upstream pressures discussed in this section is limited to 0.6–2 bar, and the upper limit of the post-throttling temperature is 1.5 K.

Fig. 9 shows the influence of P_U on q_M and q_S under the condition that $T_{pre} = 4.2$ K, $T_M = 10$ mK, and $P_D = 179$ Pa. The left side of the vertical dotted line in Fig. 9 corresponds to the situation where $P_U < P_C$ and η is assumed as 100% in this case. With the increasing P_U , q_S increases monotonically, while q_M first decreases and then increases because q_M is related to both q_S and the inlet enthalpy h_1 . When P_U first increases, the decreasing trend of h_1 cannot be offset by the opposite trend of q_S ,

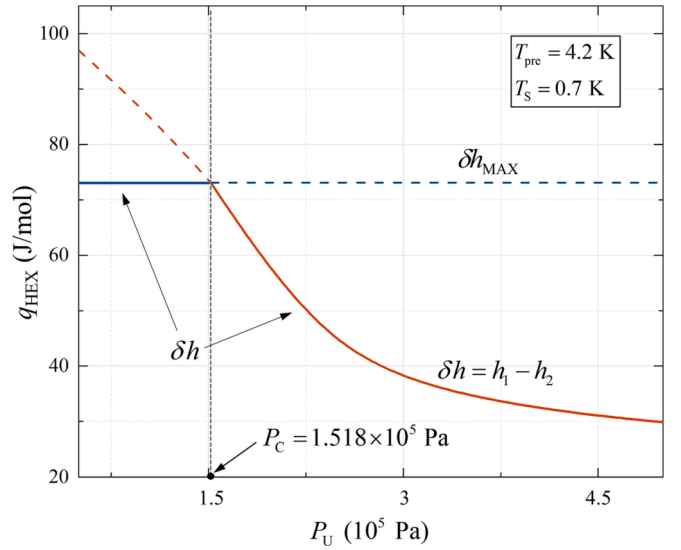


Fig. 8. Relationship between P_U and the heat exchange capacity of the first-stage CHEX.

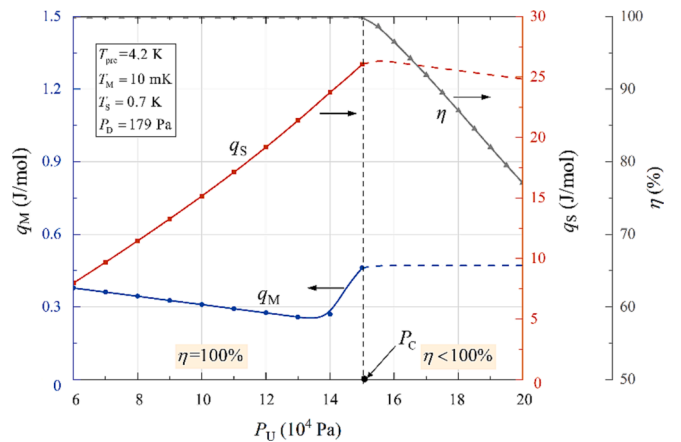


Fig. 9. Variations of q_M and q_S with P_U (the dotted lines stand for the situation of $\eta < 100\%$, and the corresponding efficiency is also shown).

resulting in a slight decline of q_M . However, when P_U keeps increasing to a particular value, h_1 will decrease rapidly and exceed the growth of q_s , leading to the sharply rising q_M . The above analyses originate from the specific properties of ^3He at extremely low temperatures.

In addition, the other side of the vertical dotted line in Fig. 9 represents $P_U > P_C$. In this case, as discussed at the beginning of Section 4, the efficiency of the first-stage CHEX cannot theoretically reach 100 %, and the reason why it is indicated by the dotted line is that the required η to ensure the outlet flow of heat exchanger to achieve 0.7 K at different pressures varies. As shown in Fig. 9, q_M keeps constant while q_s decreases slightly with the further increase of P_U . The former is mainly due to the limitation of the outlet temperature of the first-stage CHEX. On the other hand, the enthalpy of the high-pressure inlet of the still is proportional to P_U , but the heat absorbed by evaporation of ^3He on the low-pressure side is fixed. Consequently, q_s gradually declines.

4.1.2. Gross cooling capacity Q_M

With the molar flow rate taken into consideration, the variations of Q_M and Q_S of DR with P_U are shown in Fig. 10. When $P_U < P_C$, with the increasing P_U , Q_S presents a parabolic increase, which is impacted by both the increasing molar flow rate \dot{n} and q_s . However, the changing trend of Q_M is not the same as that of q_M . It increases first slightly and then sharply because \dot{n} is proportional to P_U , and its growing trend is much greater than the decrease of q_M at a lower P_U , which indicates the crucial role of \dot{n} in the DR. When $P_U > P_C$, the effect of \dot{n} on Q_M and Q_S is still dominant so both of them show a monotonically rising trend with P_U .

It is observed that Q_M keeps increasing with P_U . However, as shown in Fig. 9, when P_U increases more than P_C , the growing Q_M is obtained at the cost of heat exchanger efficiency. Assuming that the outlet temperature of the first-stage CHEX is kept at 0.7 K, as P_U rises from 1.55×10^5 Pa to 2×10^5 Pa, the corresponding maximum η declines from 98.6 % to 77.1 %, which is unreasonable for a CHEX at the extremely low temperatures, so this section is represented with a dotted line. Given a perfect heat exchanger with the efficiency of 100 %, the optimal upstream pressure $P_{U,opt}$ at a T_{pre} of 4.2 K is 1.518×10^5 Pa and Q_M reaches a maximum value of 69.7 μW .

4.2. Effects of the precooling temperature

Besides P_U , T_{pre} is also an important factor influencing the cooling performance of the DR. Fig. 11 shows the state change of the c-phase and d-phase at different T_{pre} with a P_U of 1.518×10^5 Pa.

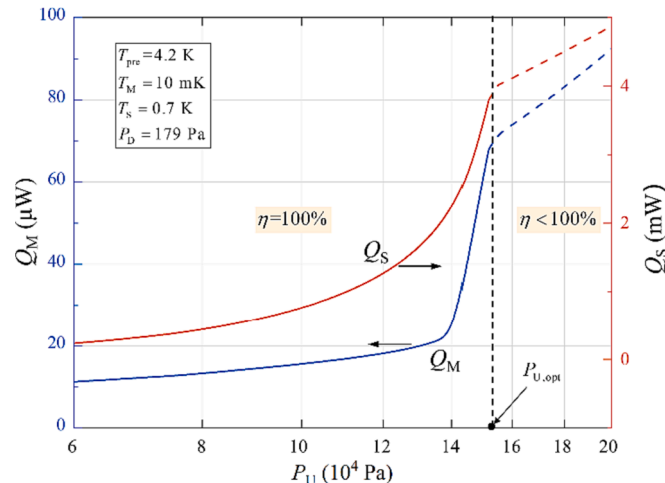


Fig. 10. Variations of Q_M and Q_S with P_U .

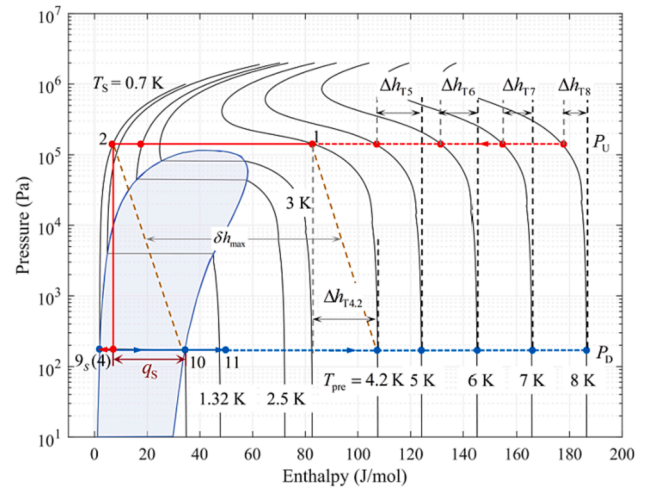


Fig. 11. Steady flow process of the c-phase and d-phase at different T_{pre} with a P_U of 1.518×10^5 Pa.

4.2.1. q_M and q_s

Fig. 12 shows the variations of q_M and q_s with T_{pre} for a series of different P_U . The dotted line indicates that η is less than 100 % and is not a constant value, so it will not be discussed in this section. For a constant P_U , q_M and q_s are both inversely proportional to T_{pre} because the cooling capacity provided by the working fluid on the low-pressure side of the first-stage CHEX keeps constant and a higher T_{pre} leads to the inadequate cooling of the working fluid on the other side. Furthermore, $T_{pre,opt}$ corresponding to the maximum q_M rises with the increase of P_U . It is noted that the maximum q_M is independent of P_U due to the opposite trends of q_s and h_1 with P_U .

Based on the above analyses, it is concluded that $T_{pre,opt}$ and $P_{U,opt}$ are in correspondence with each other in the DR. Therefore, the inflating volume can be adjusted according to the given T_{pre} during the actual operation in order to achieve the $P_{U,opt}$ under steady operation so that Q_M is maximized.

4.2.2. Gross cooling capacity

Similarly, with the molar flow rate taken into consideration, the relationship between P_U , T_{pre} and Q_M is discussed in this section. During the operation of the DR, T_{pre} , other than P_U , is usually the given parameter so the following discussion is about the optimization of P_U at different T_{pre} to improve the cooling performance of the DR.

Fig. 13 shows the effects of P_U on Q_M (a) and Q_S (b) for different T_{pre} . Given a constant T_{pre} , the trends of Q_M are the same as that in Section 4.1.2. As T_{pre} increases, the curve of Q_M gradually moves up, the pressure corresponding to the inflection point of Q_M increases, and $P_{U,opt}$ corresponding to the optimal Q_M increases as well with a perfect CHEX. The grey dotted curve in Fig. 13(a) stands for the functional relationship between T_{pre} , $P_{U,opt}$ and the optimal Q_M . It should be noted that the increasing speed of Q_M tends to slow down with the increase of T_{pre} . This means although a higher T_{pre} needs a higher $P_{U,opt}$, which can obtain a larger Q_M , the increase of T_{pre} is restricted in order to make a trade-off between the increase in Q_M and the risk of leakage caused by the increase in P_U . In addition, the parabolic increase of Q_S with P_U at different T_{pre} is also shown in Fig. 13(b), and the coefficient of the parabola decreases as T_{pre} increases.

Fitting the relationship between T_{pre} , $P_{U,opt}$, the optimal Q_M is obtained as follows:

$$P_{U,opt} = b_1 + b_2 T_{pre} + b_3 T_{pre}^2 + b_4 T_{pre}^3 \quad (44)$$

$$Q_{M,opt} = c_1 + c_2 T_{pre} + c_3 P_U + c_4 T_{pre}^2 + c_5 T_{pre} P_U \quad (45)$$

where the coefficients of b_i and c_i are shown in Table. 1.

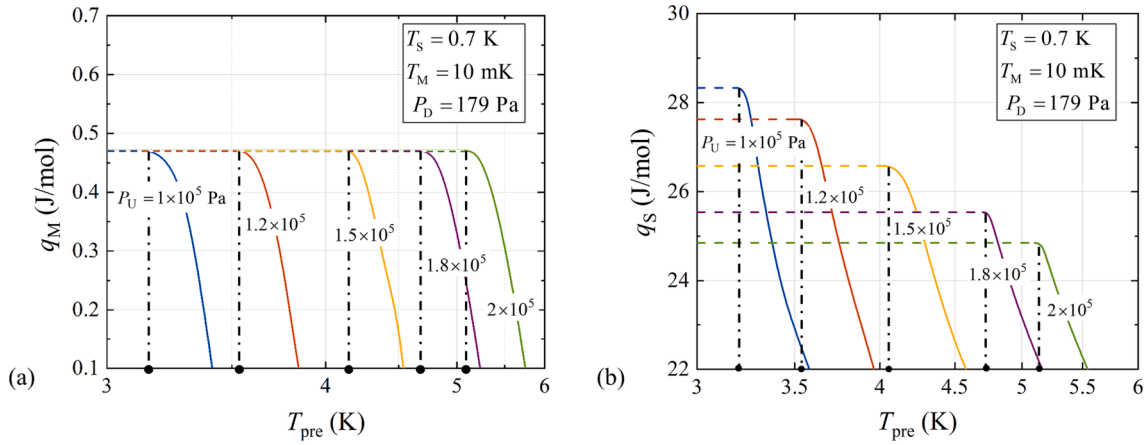


Fig. 12. Variations of q_M (a) and q_S (b) with T_{pre} for different P_U .

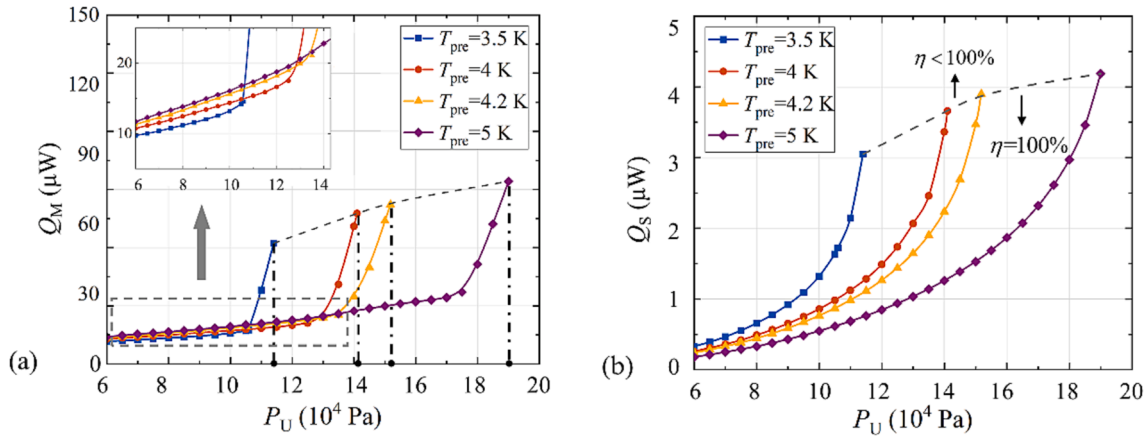


Fig. 13. Effects of P_U on Q_M (a) and Q_S (b) for different T_{pre} .

4.3. Effects of the heat exchanger efficiency

The above two sections have discussed the situation with a perfect heat exchanger. In reality, the heat exchanger efficiency is actually another important factor affecting the cooling performance of the DR. There always exist certain temperature differences between the warm and cold end of the CHEX, thereby leading to a higher temperature at the outlet. It results in not only the deviation of the corresponding enthalpy but also the influence on the molar flow rate, which makes it impossible to achieve $Q_{M,opt}$ under $P_{U,opt}$. Consequently, it is also necessary to investigate the effect of efficiency on the cooling performance under different T_{pre} and $P_{U,opt}$ when $T_S = 0.7$ K and $T_M = 10$ mK.

Fig. 14 shows the influence of the first-stage CHEX efficiency η on the temperature differences between the hot and cold ends for different T_{pre} . Due to the insufficient heat exchange between the hot and cold fluids, as the efficiency decreases, T_2 increases while T_{11} decreases, and the temperature difference at the cold end is greater than that at the warm end. Besides, when the efficiency keeps constant, the temperature variations at either the cold or warm end increase with the increasing T_{pre} due to the more inadequate heat transfer. Generally, the efficiency of the CHEX is required to be higher than 97 %.

Figs. 15–16 show the effects of efficiency on the absolute and relative reductions of the actual cooling capacity Q_M for different T_{pre} and the corresponding $P_{U,opt}$. As discussed above, Q_M increases with T_{pre} under the CHEX efficiency of 100 %. However, the decrement of Q_M caused by the reduction in the efficiency increases with the increase of precooling temperature. When the efficiency reduces from 100 % to 97 %, Q_M decreases by 34 %, 41 %, and 57 % for a T_{pre} of 3.5 K, 4 K, and 5 K,

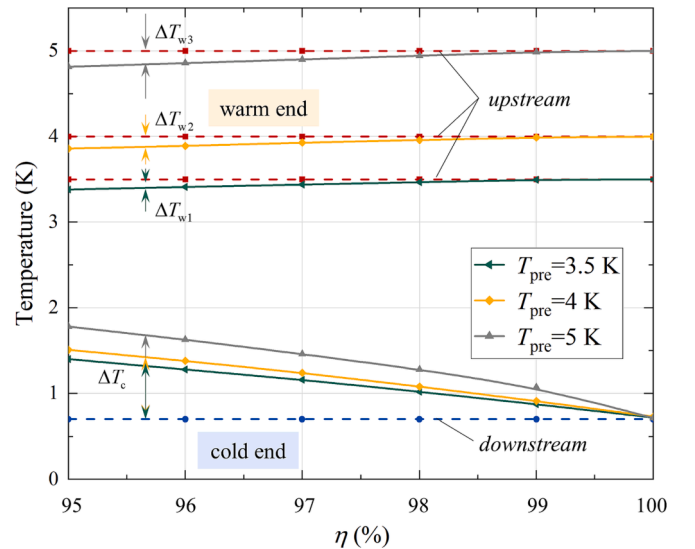


Fig. 14. Effects of the first-stage CHEX efficiency η on the temperature differences between hot and cold ends for different T_{pre} .

respectively, indicating that the decline of the efficiency has an important influence on the cooling performance of the DR, which becomes more evident at the higher T_{pre} . Given an efficiency of 97 %, Q_M is optimized to be 38.5 μ W under $T_{pre} = 4$ K and $P_{U,opt} = 1.41 \times 10^5$ Pa.

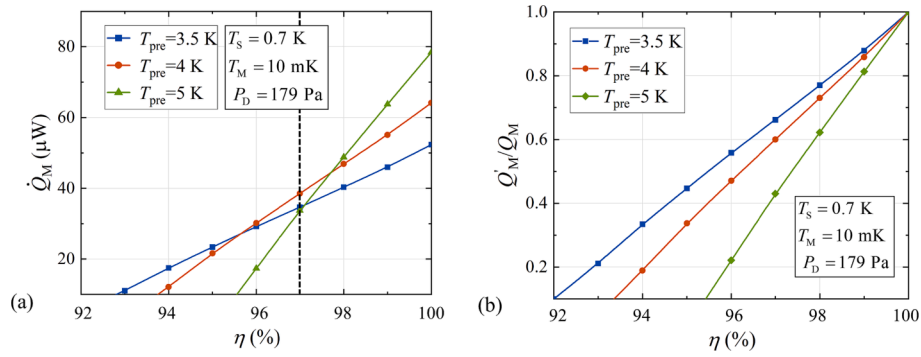


Fig. 15. Relationship between actual Q_M (a), its relative reduction (b) and the efficiency at different T_{pre} .

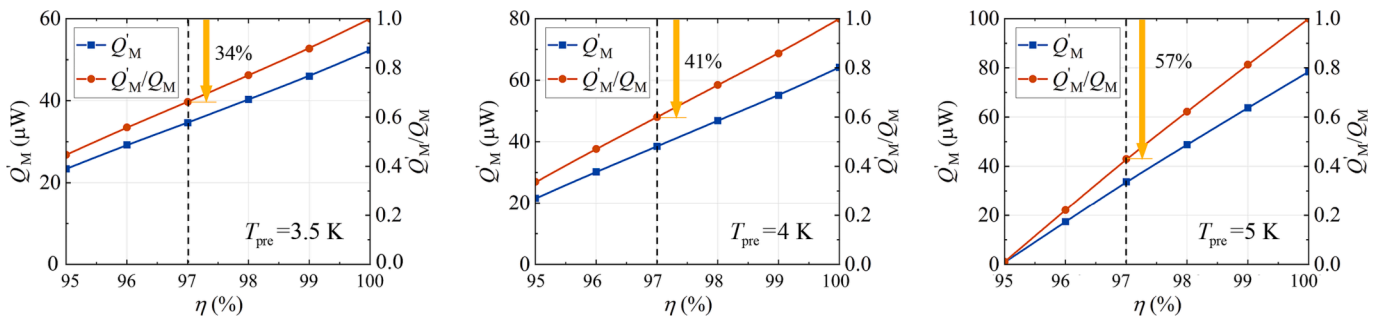


Fig. 16. Relative reduction of the actual Q_M at different precooling temperatures when $\eta = 97\%$.

5. Conclusions

The dilution refrigerator (DR) plays an important role in providing appropriate cryogenic environment for the quantum information technology and the low-temperature physics. It is necessary to carry out in-depth study of the operating mechanism of the DR and of the effects of various parameters to achieve the desired performance optimization.

This paper puts forward a simplified method to obtain the enthalpy of the ^3He - ^4He mixture using the definition of the osmotic pressure, and then builds an enthalpy flow model of the DR based on the first law of thermodynamics. The variations of the specific cooling capacity, specific still heating power and gross cooling capacity with the precooling temperature and upstream pressure are studied in the model. Then the effect of the first-stage heat exchanger efficiency is also further analyzed under the cooling temperature of 10 mK and the still temperature of 0.7 K. Some meaningful conclusions have been reached as follows:

- (1) The d -phase mixture below 0.7 K can be regarded as the ^3He flowing in the ^4He environment, and the osmotic pressure of ^3He in ^4He be done as the static pressure. The enthalpy of each state point of the c -phase and d -phase in the dilution cycle is obtained from the calculated osmotic pressure, which is applied in the subsequent thermodynamic analysis.
- (2) Given a precooling temperature, there always exists an optimal upstream pressure which maximizes the gross cooling capacity. Besides, the optimal upstream pressure and the maximum cooling capacity can be achieved by the fitting functions of the precooling temperatures. Meanwhile, the required still heating power is also the highest.
- (3) With a perfect CHEX, a higher precooling temperature results in a corresponding increase in the optimal upstream pressure, leading to an increment in both the flow rate and the gross cooling capacity. However, the coupled equations about the precooling temperature, optimal upstream pressure, and corresponding cooling capacity show that the increasing trend of cooling

capacity gradually flattens out as the precooling temperature rises, which hinders the improvement of the cooling performance.

With an imperfect CHEX, the increase in the precooling temperature leads to a sharper decline of the gross cooling capacity resulting from the decreasing heat exchanger efficiency. When the efficiency of the first-stage heat exchanger reduces from 100 % to 97 %, the cooling capacity decreases by 34 %, 41 %, and 57 % at the precooling temperature of 3.5 K, 4 K, and 5 K, respectively, indicating that the heat exchanger efficiency plays a vital role in affecting the DR performance.

- (4) To investigate the cooling performance of the DR close to the real situation, given the heat exchanger efficiency of 97 %, the maximum cooling capacity of 38.5 μW is obtained with the precooling temperature of 4 K and the upstream pressure of 1.41×10^5 Pa.

The study in this paper will provide a helpful theoretical guidance for the performance optimization of the DR.

CRediT authorship contribution statement

Yujia Zhai: Conceptualization, Methodology, Data curation, Writing – original draft. **Haizheng Dang:** Conceptualization, Methodology, Supervision, Writing – original draft, Writing – review & editing.

Declaration of Competing Interest

The authors declare that they have no known competing financial interests or personal relationships that could have appeared to influence the work reported in this paper.

Data availability

Data will be made available on request.

Acknowledgements

This work is supported by the National Natural Science Foundation of China (Grant No. 52076210), the Major Project of Science and Technology Commission of Shanghai Municipality (Grant No. 22511100100), the Collaborative Innovation Project of Shanghai Municipality (Grant No. XTCX-KJ-2023-58) and Shanghai Municipal Science and Technology Major Project (Grant No. 2019SHZDZX01).

References

- [1] Pan W, Xia JS, Stormer HL, et al. Experimental studies of the fractional quantum Hall effect in the first excited Landau level. *Phys Rev B* 2008;77(7):075307.
- [2] de-Picciotto R, Reznikov M, Heiblum M, et al. Direct observation of a fractional charge. *Phys B Condens Matter* 1998;249–251:395–400.
- [3] Mourik V, Zuo K, Frolov SM, et al. Signatures of majorana fermions in hybrid superconductor-semiconductor nanowire devices. *Science* 2012;336(6084):1003–107.
- [4] Arute F, Arya K, Babbush R, et al. Quantum supremacy using a programmable superconducting processor. *Nature* 2019;574(7779):505–10.
- [5] Tuckerman DB, Hamilton MC, Reilly DJ, et al. Flexible superconducting Nb transmission lines on thin film polyimide for quantum computing applications. *Supercond Sci Technol* 2016;29(8):084007.
- [6] Shirron PJ. Cooling capabilities of adiabatic demagnetization refrigerators. *J Low Temp Phys* 2007;148:915–20.
- [7] <https://bluefors.com/products/xldsl-dilution-refrigerator/>.
- [8] <https://nanoscience.oxinst.com/products/proteox5mk>.
- [9] Wheatley JC. Dilute solutions of ^3He in ^4He at low temperature. *Am J Phys* 1968;36(3):181–210.
- [10] Wheatley JC, Vilches OE, Abel WR. Principles and methods of dilution refrigeration. *Physics Physique Fizika* 1968;4(1):1–64.
- [11] Radebaugh R, Siegwarth JD. Dilution refrigerator technology. *Cryogenics* 1971;11(5):368–84.
- [12] Radebaugh R. Very-low-temperature cooling systems. In: Walker G, editor. *Cryocoolers*. Springer Science+Business Media, LLC; 1983. p. 177–251.
- [13] Lounasmaa OV. Dilution refrigeration. *J Phys E Sci Instrum* 1979;12(8):668.
- [14] Frossati G. Obtaining ultralow temperatures by dilution of ^3He into ^4He . *J Phys Colloques* 1978;39(C6). C6–1578-C6-89.
- [15] Pradhan J, Das NK, Chakraborty A. Thermo-dynamical process simulation of dilution refrigerator. *Cryogenics* 2013;57:158–65.
- [16] Pradhan J, Das NK, Chakrabarti A. Transient phenomena initiating phase transition in dilution refrigerator. *Cryogenics* 2014;63:69–76.
- [17] Chaudhry G, Volpe A, Camus P, et al. A closed-cycle dilution refrigerator for space applications. *Cryogenics* 2012;52:471–7.
- [18] Mueller BW, Miller FK. Development of a thermodynamic model for a cold cycle ^3He - ^4He dilution refrigerator. *Cryogenics* 2016;79:85–95.
- [19] Radebaugh R. Thermodynamic properties of ^3He - ^4He solutions with application to the dilution refrigerator. National Bureau of Standards; 1967.
- [20] Kuersten JGM, Castelijns CAM, de Waele ATAM, et al. Thermodynamic properties of liquid ^3He - ^4He mixtures at zero pressure for temperatures below 250 mK and ^3He concentrations below 8 %. *Cryogenics* 1985;25(8):419–43.
- [21] Chaudhry G, Brisson JG. Thermodynamic properties of liquid 3He-4He mixtures between 0.15 K and 1.8 K. *J Low Temp Phys* 2009;155(5):235–89.
- [22] Chaudhry G, Brisson JG. Thermodynamic properties of liquid 3He-4He mixtures between 0–10 bar below 1.5 K. *J Low Temp Phys* 2010;158(5):806–53.
- [23] Miller FK, Brisson JG. Measurements of the superfluid Joule-Thomson refrigerator using high concentration 3He-4He mixtures. *J Low Temp Phys* 2007;147(5):559–78.
- [24] Landau J, Tough J-T, Brubaker NR, et al. Temperature, pressure, and concentration dependence of the osmotic pressure of dilute ^3He - ^4He mixtures. *Phys Rev A* 1970;2(6):2472–82.
- [25] Huang YH, Chen GB. A practical vapor pressure equation for helium-3 from 0.01 K to the critical point. *Cryogenics* 2006;46:833–9.
- [26] Kierstead HA. Phase diagram and concentration susceptibility of ^3He - ^4He mixtures near the tri-critical point. *J Low Temp Phys* 1979;35(1):25–39.
- [27] Ahlers G, Greywall DS. Second-sound velocity and superfluid density near the tricritical point in ^3He - ^4He mixtures. *Phys Rev Lett* 1972;29(13):849–52.
- [28] Maytal BZ, Pfothenhauer JM. Miniature Joule-Thomson cryocooling; principles and practice. Berlin: Springer; 2013.
- [29] Koike Y, Morii Y, Igarashi T, et al. A dilution refrigerator using the pulse tube and GM hybrid cryocooler for neutron scattering. *Cryogenics* 1999;39(7):579–83.
- [30] Uhlig K. “Dry” dilution refrigerator with pulse-tube precooling. *Cryogenics* 2004;44(1):53–7.
- [31] Vermeulen GA, Frossati G. Powerful dilution refrigerator for use in the study of polarized liquid ^3He and nuclear cooling. *Cryogenics* 1987;27(3):139–47.